Presented as late breaking results contribution
21st IFAC World Congress (Virtual)
Berlin, Germany, July 12-17, 2020

Model-free control for machine tools

Jorge Villagra * **Cédric Join** **,**** **Rodolfo Haber** *
Michel Fliess ***,****

* *Centre for Automation and Robotics (CSIC-UPM), 28500 Arganda del Rey, Spain (e-mail: {jorge.villagra,rodolfo.haber}@csic.es)*
** *CRAN (CNRS, UMR 7039), Université de Lorraine, BP 239, 54506 Vandœuvre-lès-Nancy, France, (e-mail: cedric.join@univ-lorraine.fr)*
*** *LIX (CNRS, UMR 7161), École polytechnique, 91128 Palaiseau, France, (e-mail: Michel.Fliess@polytechnique.edu)*
**** *AL.I.E.N., 7 rue Maurice Barrès, 54330 Vézelise, France, (e-mail: {cedric.join, michel.fliess}@alien-sas.com)*

Abstract: Cascade P-PI control systems are the most widespread commercial solutions for machine tool positioning systems. However, friction, backlash and wearing effects significantly degrade their closed-loop behaviour. This works proposes a novel easy-to-tune control approach that achieves high accuracy trajectory tracking in a wide operation domain, thus being able to mitigate wear and aging effects.

Keywords: Machine tool, model-free control, cascade control, robustness, tracking

1. INTRODUCTION

Current automated machine tools requires high-accuracy positioning of their working axes. Several mechanical effects, often hard to identify, may compromise the appropriate positioning of the machine end-tool, thus degrading the finishing quality. To ensure that tolerances are maintained, the machine drives are equipped with tracking controllers that aims at efficiently compensate the nonlinear behaviour of the axes.

State-of-the-art axis-positioning solutions use P and PI cascade controllers with additional feedforward compensation (Armstrong-Hélouvry et al. (1994)), used to counteract nonlinear effects, such as friction or backlash. In most of these compensation schemes [ranging from observers (Huang et al. (2009)), to nonlinear identification (Merzouki et al. (2007)) or to evolutive algorithms (Guerra et al. (2019)), the friction model parameters are considered constant and characterized with offline identification experiments. These models significantly degrade in the presence of additional wear-related effects. As a result, the linear control loops need to be frequently re-tuned, leaving margin for more efficient strategies.

The need for achieving nominal performance even in the presence of increased friction, motivates the investigation of nonlinear control strategies. Gain-scheduling (Van de Wouw et al. (2008)), sliding-mode (Jin et al. (2009)), backstepping (Zhang and Ren (2014)) and nonlinear adaptive controllers (Papageorgiou et al. (2018)) can eventually minimize this performance deterioration, but at the expense of a significant design complexity. In addition to that, most of these techniques focus on stability of the closed-loop dynamics without emphasizing high-accuracy positioning.

The contribution of this paper is to present a novel control approach that attempts to answer the aforementioned challenges: (i) achieve high accuracy trajectory tracking, while (ii) keeping an easy-to-tune design, and (iii) being able to mitigate the wear and aging effects in the closed-loop behaviour. To that end, model-free control techniques, introduced in (Fliess and Join (2013)) and successfully deployed in a wide diversity of concrete case-studies [1] (see e.g. Fliess and Join (2013) and Bara et al. (2018) and the references therein), will be implemented and tested.

The outline of the paper is as follows. Section 2 describes the system model to be controlled, with particular emphasis on the wear-related parameters and effects. The novel control strategy is presented in Section 3, after which some selected experimental results are showed in Section 4. Finally, some concluding remark and hints on the future work are drawn in Section 5.

2. SYSTEM DESCRIPTION

The behavior of a machine tool axis can be represented by a double mass oscillator (motor and load) interconnected by a spring and a damper, as shown in Fig. 1.

The dynamics of this model are parametrized by the drive motor and generalized inertias (J_m, J_l respectively), the spring constant corresponding to the shaft stiffness K and the damping coefficient of the shaft B. The electromechanical torque and angular speed generated by the drive motor are denoted M_m and ω_m, respectively, whereas the inter-connecting torque and the angular speed of the load are respectively M_l and ω_l.

⋆ This work is partially supported by the joint CNRS (France)-CSIC (Spain) PICS Program through the project UbiMFC (CoopIntEer 203 073)

[1] Some applications are patented.

Copyright lies with the authors

Presented as late breaking results contribution
21st IFAC World Congress (Virtual)
Berlin, Germany, July 12-17, 2020

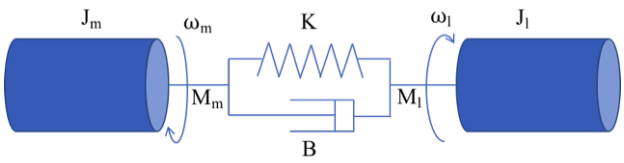

Fig. 1. Scheme of machine tool axis dynamics: double mass oscillator

The following transfer function describes the relationship between the motor rotation speed and the applied motor torque in the operational domain:

$$\omega_m(s) = B_s(s)M_m(s) = \\ = \frac{1}{J_m s} \cdot \frac{s^2 + 2D_1\omega_{0_1}s + \omega_{0_1}^2}{s^2 + 2D_2\omega_{0_2}s + \omega_{0_2}^2} M_m(s) \quad (1)$$

where $\omega_{0_1} = \sqrt{\frac{K}{J_l}}$, $\omega_{0_2} = \omega_{0_1}\sqrt{1 + \frac{J_l}{J_m}}$, $D_1 = \frac{B\omega_{0_2}}{2K}$ and $D_2 = \frac{B}{2\omega_{0_1}J_l}$. The dynamics of this system depend essentially on the inertia of the motor and the load, as well as on the configuration of the spring-damper system. Note that in the absence of friction the damping coefficients (D_1, D_2) and the natural frequencies ($\omega_{0_1}, \omega_{0_2}$) are interrelated:

$$\omega_{0_1} = 2\pi f_1, \omega_{0_2} = \left(\frac{J_m + J_l}{J_m}\right)^{1/2} \omega_{0_1}, D_2 = \left(\frac{J_m + J_l}{J_m}\right)^{1/2} D_1$$

and that we can consider $f_1 = \frac{\omega_{0_1}}{2\pi}$ and D_1 as the independent parameters which influence the whole dynamics of the system. The aging and wear effects will be modelled so that these 2 variables can take values in a broad operational domain, representative of commercially available machines nowadays: $30 \leq f_1 \leq 70$, $0.08 \leq D_1 \leq 0.15$

The relationship between the rotation speed at the load ω_l and at the motor ω_m can also be expressed in the operational domain as follows:

$$\omega_l(s) = C_s(s)\omega_m(s) = \frac{2D_1\omega_{0_1}s + \omega_{0_1}^2}{s^2 + 2D_1\omega_{0_2}s + \omega_{0_1}^2}\omega_m(s) \quad (2)$$

Furthermore, the current i_r can be connected with the motor torque M_m while neglecting the dynamics of the electrical system with the following expression:

$$M_m(s) = A_s(s)i_r(s) = \frac{K_t}{J_m s} i_r(s) \quad (3)$$

where K_t is the electric torque constant. The current at the motor $i(t)$ has losses compared to the one generating torque i_r, which can be written as follows:

$$i_r(t) = i(t) - i_f(t) \quad (4)$$

where i_f expresses the current needed to overcome the friction as a function of the load angular speed:

$$i_f(t) = D_s(\omega_l(t)) = \frac{1}{K_t}\left(F_c sgn(\omega_l(t)) + F_v\omega_l(t)\right) \quad (5)$$

being F_c and F_v the Coulomb and viscous friction coefficients, respectively. Note also the existence of a backlash effect on the load which can play a significant role during the reversal phases of the control signal.

Fig. 2 depicts the dependencies between expressions (1) - (5) and their interactions with the two control loops C_0, C_1which are detailed in the following section.

3. MODEL-FREE APPROACH FOR DRIVE-TRAINS

3.1 Cascade P-PI control

A widely accepted control structure in the industry is a cascade with 2 loops: (i) an external one on the position of the load, where typically a proportional corrector is used, and (ii) an internal one on the speed of the motor, where a PI is often implemented. The outer loop u_1 is closed using a feedforward term $C_{0_{ff}}$ and a feedback term $C_{0_{fb}}$:

$$u_1(t) = C_0\left(\theta_l(t)\right) = C_{0_{ff}}(t) + C_{0_{fb}}(\theta_l(t)) = \\ = \dot{\theta}_l^*(t) + \Phi_1\left(\theta_l^*(t) - \theta_l(t)\right) \quad (6)$$

where $\theta_l^*(t)$ is the load position reference trajectory and Φ_1 is a generic corrector applied to the load position error. The inner control loop is also a combination of feedforward $C_{1_{ff}}$ and feedback $C_{1_{fb}}$:

$$u_2(t) = C_1\left(\omega_m(t)\right) = C_{1_{ff}}(t) + C_{1_{fb}}(\omega_m(t))) = \\ = \frac{Jm + Jl}{Kt}\dot{\omega}_l^*(t) + \Phi_2\left(\omega_m^*(t) - \omega_m(t)\right), \ \omega_m^*(t) = u_1(t) \quad (7)$$

where $\omega_m^*(t)$ is the reference trajectory for the motor speed which, given the cascade structure of Fig. 2, is equal to the external loop control variable $u_1(t)$. The term Φ_2 represents a generic corrector applied to the engine speed error. Note that in the case of a P-PI scheme $\Phi_1 = K_{p_o}e$ and $\Phi_2 = K_{p_i}e + K_{i_i}\int edt$

3.2 Model-free control principles

Model-free controllers are used in this work because they combine the well-known and easy-to-tune PID structure with an "intelligent" term that compensates the effects of nonlinear dynamics, disturbances or uncertain parameters.

As demonstrated in (Fliess and Join (2013)), most SISO systems can be written locally as

$$\dot{y} = F + \alpha u \quad (8)$$

where $\alpha \in \mathbb{R}$ is a constant parameters, which do not necessarily represent a physical magnitude, and whose value is chosen by the practitioner such that it allows F and αu to be of the same order of magnitude.

The data-driven term F, which includes not only the unknown structure of the system but also any disturbance (Fliess and Join (2013)), is computed as follows:

$$\hat{F}(t_k) = \hat{\dot{y}}(t_k) - \alpha u(t_{k-1}) \quad (9)$$

Taking the above into consideration, the loop can be closed with an intelligent controller (iP) using the following expression:

$$u = K_p e + \frac{\dot{y}^* - \hat{F}}{\alpha} \quad (10)$$

where y^* is the reference trajectory, $e = y - y^*$ is the tracking error and $K_P \in \mathbb{R}$ is a gain. Note that the tuning complexity of this approach is comparable to a PI controller, as only 2 parameter need to be chosen.

Presented as late breaking results contribution
21st IFAC World Congress (Virtual)
Berlin, Germany, July 12-17, 2020

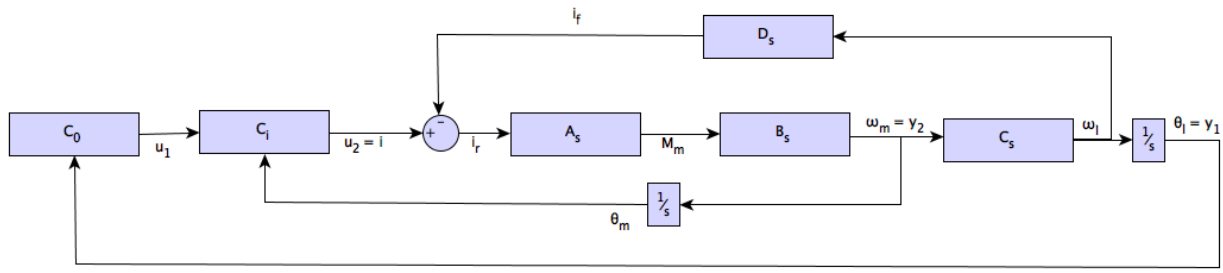

Fig. 2. Block diagram of the machine tool control structure

3.3 Cascade model-free control

The classic P-PI structure is replaced by another scheme based on a iP-iP structure, where the following outer and an inner input-output model are used (see Lafont et al. (2015) for an explanation for such MIMO systems):

$$\dot{y}_1 = F_1 + \alpha_1 u_1,\ \dot{y}_2 = F_2 + \alpha_2 u_2$$

where inputs u_1, u_2 and outputs $y_1 = \theta_l, y_2 = \omega_m$ corresponds to the signals represented in Fig. 2, and $\alpha_1, \alpha_2 \in \mathbb{R}$ are gains chosen by the control engineer.

Following the expression of a generic iP presented in (10), the outer and inner loops are respectively closed with feedback controllers Φ_1^* and Φ_2^* to which feedforward terms $C_{0_{ff}} = \dot{\theta}_l^*$ and $C_{1_{ff}} = \dfrac{Jm + Jl}{Kt}\dot{\omega}_l^*$, introduced in (6) and (7), are respectively added as follows:

$$\begin{aligned} u_1(t) &= C_0\left(\theta_l(t)\right) = \dot{\theta}_l^*(t) + \Phi_1\left(\theta_l^*(t) - \theta_l(t)\right), \\ \Phi_1^* &= K_{p_o}^*\left(\theta_l^*(t) - \theta_l(t)\right) + \frac{1}{\alpha_1}\left(\dot{\theta}_l^* - \hat{F}\right) \end{aligned} \tag{11}$$

$$\begin{aligned} u_2(t) = C_1\left(\omega_m(t)\right) &= \frac{Jm + Jl}{Kt}\dot{\omega}_l^*(t) + \Phi_2\left(\omega_m^*(t) - \omega_m(t)\right) \\ \Phi_2^* &= K_{p_i}^* e_m + \frac{1}{\alpha_2}\left(\dot{\omega}_m^* - \hat{F}\right), \\ e_m &= \omega_m^*(t) - \omega_m(t),\ \omega_m^*(t) = u_1(t) \end{aligned} \tag{12}$$

where $K_{p_o}^*$ and $K_{p_i}^*$ are the proportional gains of the outer and inner iP, respectively.

4. EXPERIMENTAL RESULTS

The P-PI cascade controller and the model-free iP-iP control system, expressed respectively in (6)-(7) and in (11)-(12) have been thoroughly compared. To that end, a benchmark reference trajectory has been selected (see Fig 3a), where several inversions zones challenge the control system.

To quantitatively compare both control approaches, the following 2 key performance indicators have been chosen:

$$ITAE = \int_0^T t|\theta_l - \theta_l^*|dt,\ IAU = \int_0^T |u|dt$$

which will be computed considering the whole testing interval $t \in [0, 10]$.

Fig. 3b and Table 1 allow to see and quantify the behaviour of each strategy. In both elements, 4 different control

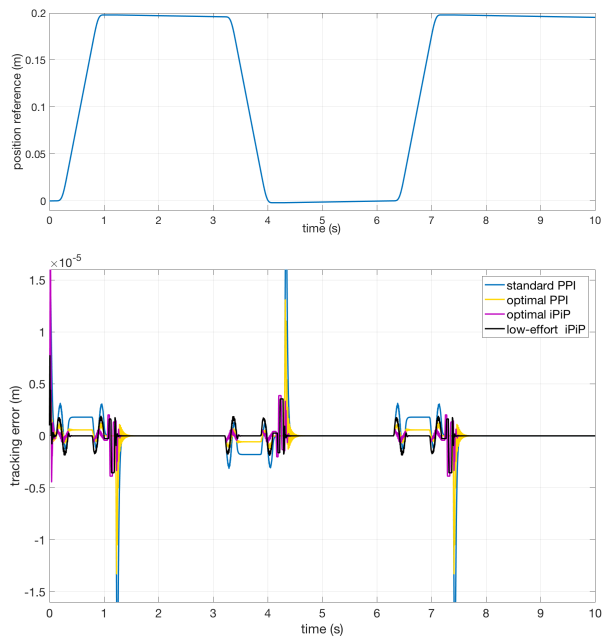

Fig. 3. a) Load reference trajectory; b) Tracking error

configurations have been analysed for a system with significantly different dynamic behaviour (in configuration Σ_1, $D_1 = 70, f_1 = 0.15$, while in Σ_2, $D_1 = 30, f_1 = 0.08$):

(1) a P-PI, whose gains $(K_{p_o}, K_{p_i}, K_{i_i})$ are obtained from a commercial control system for machine tools
(2) a P-PI, whose gains $(K_{p_o}, K_{p_i}, K_{i_i})$ have been optimised with respect to criteria $\mathcal{J} = ITAE + w_u * IAU$ for a specific operation condition
(3) an iP-iP, whose gains $(\alpha_1, \alpha_2, K_{p_o}^*, K_{p_i}^*)$ have been optimized with respect to the same criteria and for the same specific operation condition
(4) an iP-iP identically tuned, but incorporating a model-based feedforward (FF).

Note that the last control variant introduces an anticipatory control term:

$$C_{ff}(s) = \frac{s^2 + 2D_2\omega_{0_2}s + \omega_{0_2}^2}{s^2 + 2D_1\omega_{0_1}s + \omega_1^2}\omega_l^*(s) \tag{13}$$

which presumes D_1 and f_1 well know, which is not often the case, unless off-line identification tests have been conducted. The motivation to include this term is to reduce the control effort generated by iP-iP controllers. However, as the involved parameters may be badly known, a fifth item to be compared has been introduced in Table

Presented as late breaking results contribution
21st IFAC World Congress (Virtual)
Berlin, Germany, July 12-17, 2020

Table 1. Comparison of PPI and iPiP under different operation conditions

		P-PI nom	P-PI nom opt	iP-iP	iP-iP+FF	iP-iP+FF (wrong param.)
$\Sigma_1(D_1 = 70, f_1 = 0.15)$	ITAE	$2.978 \cdot 10^{-5}$	$1.024 \cdot 10^{-5}$	$\mathbf{6.823 \cdot 10^{-6}}$	$9.554 \cdot 10^{-6}$	$9.598 \cdot 10^{-6}$
	IAU	5.360	5.366	6.221	**5.162**	5.162
$\Sigma_2(D_1 = 30, f_1 = 0.08)$	ITAE	$7.319 \cdot 10^{-2}$	$3.134 \cdot 10^{-4}$	$\mathbf{1.680 \cdot 10^{-4}}$	$1.913 \cdot 10^{-4}$	$1.944 \cdot 10^{-4}$
	IAU	119.6	5.731	5.456	**5.343**	5.345

1, aiming at assessing the sensitivity of the closed-loop behaviour to wrong values of D_1 and f_1 (0.15 and 70 instead of 0.08 and 30, and viceversa).

As can be observed, the iP-IP controller achieves a significant improvement both with respect to the standard and the optimised P-PI, both quantitatively -see ITAE- and qualitatively -lower inversion peaks. Although the control action is higher in the regular iP-iP control, the inclusion of an anticipative model not only mitigates this aspect, but it even achieves a lower tracking error than P-PI.

A key consideration of this work is the assessment of model-free controllers under a significant variation of wear related-parameters, namely D_1 and f_1. To that end, a Monte-Carlo simulation has been conducted using normal distributions of such parameters, as depicted in Fig. 4, where the desired operating domains have been approximated by conservative normal distributions $f_1 \sim \mathcal{N}(55, 4)$ and $D_1 \sim \mathcal{N}(0.13, 0.01)$.

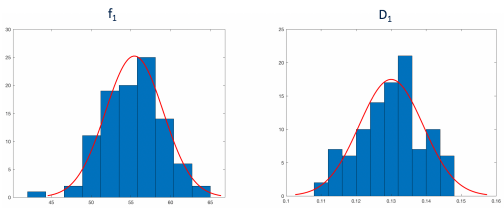

Fig. 4. Histograms with generated values of f_1 and D_1

The existing control approaches have difficulty in obtaining good behavior in these ranges, which limits the field of operation to a very restricted set of machines.

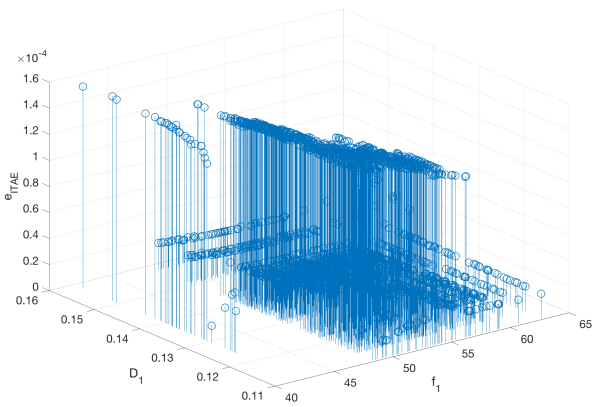

Fig. 5. Stem representation of the Monte-Carlo test, with $f_1 \sim \mathcal{N}(55, 4)$ and $D_1 \sim \mathcal{N}(0.13, 0.01)$

Fig. 5 represents the difference in terms of ITAE between the standard P-PI and the iP-iP control structures for the generated input parameter combinations. The values are positive in every tested case, showing that iP-iP provides also more accurate positioning than P-PI when wearing effects appear.

5. CONCLUDING REMARKS

An easy-to-tune model-free control approach has been presented for axis-positioning in machine tool systems. The preliminary results of this work exhibits an outstanding tracking behaviour not only under a specific operation condition, but also when a significant wear-induced parameter range is considered.

REFERENCES

Armstrong-Hélouvry, B., Dupont, P., and De Wit, C.C. (1994). A survey of models, analysis tools and compensation methods for the control of machines with friction. *Automatica*, 30(7), 1083–1138.

Bara, O., Fliess, M., Join, C., Day, J., and Djouadi, S.M. (2018). Toward a model-free feedback control synthesis for treating acute inflammation. *Journal of Theoretical Biology*, 448, 26–37.

Fliess, M. and Join, C. (2013). Model-free control. *International Journal of Control*, 86(12), 2228–2252.

Guerra, R.H., Quiza, R., Villalonga, A., Arenas, J., and Castaño, F. (2019). Digital twin-based optimization for ultraprecision motion systems with backlash and friction. *IEEE Access*, 7, 93462–93472.

Huang, W.S., Liu, C.W., Hsu, P.L., and Yeh, S.S. (2009). Precision control and compensation of servomotors and machine tools via the disturbance observer. *IEEE Transactions on Industrial Electronics*, 57(1), 420–429.

Jin, M., Lee, J., Chang, P.H., and Choi, C. (2009). Practical nonsingular terminal sliding-mode control of robot manipulators for high-accuracy tracking control. *IEEE Trans. on Industrial Electronics*, 56(9), 3593–3601.

Lafont, F., Balmat, J.F., Pessel, N., and Fliess, M. (2015). A model-free control strategy for an experimental greenhouse with an application to fault accommodation. *Computers and Electronics in Agriculture*, 110, 139–149.

Merzouki, R., Davila, J., Fridman, L., and Cadiou, J. (2007). Backlash phenomenon observation and identification in electromechanical system. *Control Engineering Practice*, 15(4), 447–457.

Papageorgiou, D., Blanke, M., Niemann, H.H., and Richter, J.H. (2018). Friction-resilient position control for machine tools—adaptive and sliding-mode methods compared. *Control Engineering Practice*, 75, 69–85.

Van de Wouw, N., Pastink, H., Heertjes, M.F., Pavlov, A.V., and Nijmeijer, H. (2008). Performance of convergence-based variable-gain control of optical storage drives. *Automatica*, 44(1), 15–27.

Zhang, Y. and Ren, X. (2014). Adaptive backstepping control of dual-motor driving servo systems with friction. In *Sixth Int. Conference on Intelligent Human-Machine Systems and Cybernetics*, volume 1, 214–217.